International Journal of Technology

http://ijtech.eng.ui.ac.id

Research Article

Machinability of the Stepped Cylindrical Electrode in the Electrical Discharge Machining

Kamonpong Jamkamon[1], Pichai Janmanee[1], Niwat Mookam[2], Suppawat Chuvaree[1*]

[1]Department of Mechanical and Industrial Engineering, Faculty of Engineering, Rajamangala University of Technology Krungthep, Bangkok 10120, Thailand

[2]Department of Industrial and Production Engineering, Faculty of Engineering, Rajamangala University of Technology Rattanakosin Wang Klai Kangwon Campus, Huahin, Prachuapkhirikhan 77110, Thailand

[*]Corresponding author: suppawat.c@mail.rmutk.ac.th, Tel.: +6622879600 (2484)

Abstract: In this study, we investigated a modified electrode with a stepped cylindrical shape to improve machinability in the electrical discharge machining process. A stepped cylindrical electrode with varied land heights and shank sizes was designed. A copper electrode was used to drill holes at a machining depth of 45 mm on the tool steel. The results revealed that the material removal rate of the shoulder and relief angle designs increased by 277.54% and 269.91%, respectively, compared with those of a conventional electrode for a land height of 0.90 mm. The material removal rate decreased slightly with increasing land height for both electrode designs. The electrode wear ratio of all modified electrodes was less than 1%, and the lowest electrode wear ratio of approximately 0.45% was observed at a land height of 2.25 mm. In addition, the diameter of the drilled hole along the machining depth was greatest in the middle. The concave shape on the side wall of the drilled hole for the modified electrode was lower than that of the conventional tool. The concave shape of the drilled hole was drastically reduced with a sufficient decrease in the land height and shank size of the modified electrode. This was due to the lower area on the sidewall between the electrode and the drilled hole, with the stepped cylindrical design leading to easy elimination of debris particles from the sparking area and improved machining performance. Therefore, the machinability of the stepped cylindrical electrode was greater than that of the conventional machining.

Keywords: Debris particles; Electrical discharge machining; Material removal rate; Stepped cylindrical electrode

1. Introduction

Electrical discharge machining (EDM) is a contemporary method for removing work material by means of serial discharges on an electrically conductive workpiece and tool electrode (Mao et al., 2020; Ni et al., 2017). The EDM process removes a part of the work material using the temperature produced by electrical discharge to erode the material with the aid of dielectric fluid flushing (Kumar and Singh, 2018). The discharge current induces an electrical spark through the dielectric medium, without any contact between the tool electrode and the workpiece. The thermal energy produced removes the work material by melting and evaporating erosion within a short period and specific regions. Consequently, EDM is a widely used method for machining workpieces because the mechanical properties of the work material are negligible because of the cutting instrument's noncontact nature during the machining process (Kumar and Singh, 2019). AISI P20 tool steel contains chromium and nickel, which contribute to the hardness of the material. This material is widely used in injection molds and casting dies because of its superior wear resistance, consistent structure, high hardness, and reasonable high-temperature strength. EDM is one of the most popular machining processes for manufacturing

https://doi.org/10.14716/ijtech.v17i2.7979
Received July 2025; Revised October 2025; Accepted February 2026

complex shapes in injection molding (Priyadarshini et al., 2022).

Compared with conventional machining, electrical discharge machining (EDM) inherently yields a lower material removal rate (MRR) and longer cycle times, especially for hard materials. This poor efficiency is due to inadequate debris and bubble flushing. In addition, accumulated particles weaken the dielectric medium and cause short-circuiting of the discharge current, interrupting the spark and slowing material removal (Mufti et al., 2020). Researchers have explored changes in tool design, motion, and process parameters to mitigate this. For example, studies on tool steel EDM have shown that increasing the discharge current or pulse duration increases the MRR but at the cost of worse surface finish and accuracy (Aghdeab et al., 2021; Straka and Hašová, 2018). Conversely, when a fresh dielectric medium is introduced between pulses, motions that refresh the gap (electrode lifting or electrode vibration) improve stability (J. Wang et al., 2012). Many new approaches are effective. For example, adding conductive powders to the dielectric fluid enhances spark dispersion. Mookam et al., 2021 reported that mixing graphite powder greatly increased the MRR, improved the surface finish, and stabilized the process. Flushing strategies have also advanced. Ahmed et al., 2021 introduced a bottom orifice in a tubular electrode to eject debris, similar to injection-flushing techniques, which can increase the MRR by 80%. Electrode rotation is a simple yet powerful method. Dwivedi and Choudhury, 2017 reported that compared with a static tool, rotating a copper tool improved debris clearance and spark quality, increasing the MRR by approximately 40%. Similarly, shaping the electrode for self-flushing is beneficial. Rafaqat et al., 2020 designed a 10-degree relief and landed it on a cylindrical electrode, reducing the hole-drilling time by nearly half (49% reduction) and yielding much smaller radial overcut and smoother hole walls. In summary, optimized electrode geometry (land/relief, helical slots, or stepped profiles) and motion (rotation or vibration) significantly increase EDM productivity by continuously sweeping debris from the gap, which in turn increases the MRR and reduces electrode wear.

Based on a review of the literature in the past decade, many researchers have focused on the optimal machining parameters because machine adjustments have essentially improved the machining performance. In addition, mixed powder and rotating electrode techniques have been employed to improve the machining efficiency. However, these techniques require the attachment of accessories to the machine structure. The machining performance can be improved by increasing the escape area to eliminate debris particles and bubbles moving from the machining area (Wei et al., 2025; Kumar and Singh, 2019). The concentration of debris particle flow throughout the machining area reduces the dielectric fluid's insulating strength, leading to a high density of secondary sparks between the drilled hole's sidewall and tool electrode (Firat and Bozdana, 2025; Dhakar et al., 2022). These factors may affect the machining performance and integrity of the drilled holes. The assumption of a modified electrode based on an increase in the escape area and a limited region of secondary spark is expected to improve the machine performance and integrity of the machined surface. A few studies have used simple geometric electrode modification for deep holes. The modification of tool electrodes to improve machining performance is an interesting recent area of study because of the low machining cost. Therefore, the current study focused on the innovative design of a stepped cylindrical electrode for deep drilling holes with different land heights to evaluate the secondary spark and shank sizes to increase the debris and bubble movement escape area. The novelty of this work is based on the use of an electrode for flushing improvement without extra machine modifications. This study aimed to examine how the modified electrode land height and shank size for deep hole drilling affect the improvement in machinability, along with the machining time along the drilled hole depth, material removal rate, electrode wear ratio, drilled hole dimension, and machined surface roughness.

2. Materials and methods used

2.1 Experimental material

Experimental tests were conducted on an Aristech 430 CNC die sinking electrical discharge machine (Aristech, Taichung City, Taiwan) to investigate the effects of electrode design on machining. Figure 1(a) shows a schematic diagram of the experimental setup. A cylindrical copper electrode was used to machine the steel-grade AISI P20 tool. The dimensions of the workpiece with the grinding surface were 10 mm × 50 mm × 65 mm. Several plates were clamped to the fixture, which was mounted onto the working tank using a machine vise. The hole drilled by electrical discharge machining was located on the parting line of the coupled plate, as shown in Figure 1(b). The machining depth was 45 mm. The side flushing of the oil dielectric fluid (DIEL MS 7000, TOTAL) was supplied to the machining area through a nozzle and continuously recirculated to the dielectric filler tank of the electrical discharge machine. The finished machined workpiece was separated to investigate the integrity of the drilled holes, as shown in Figure 1(c).

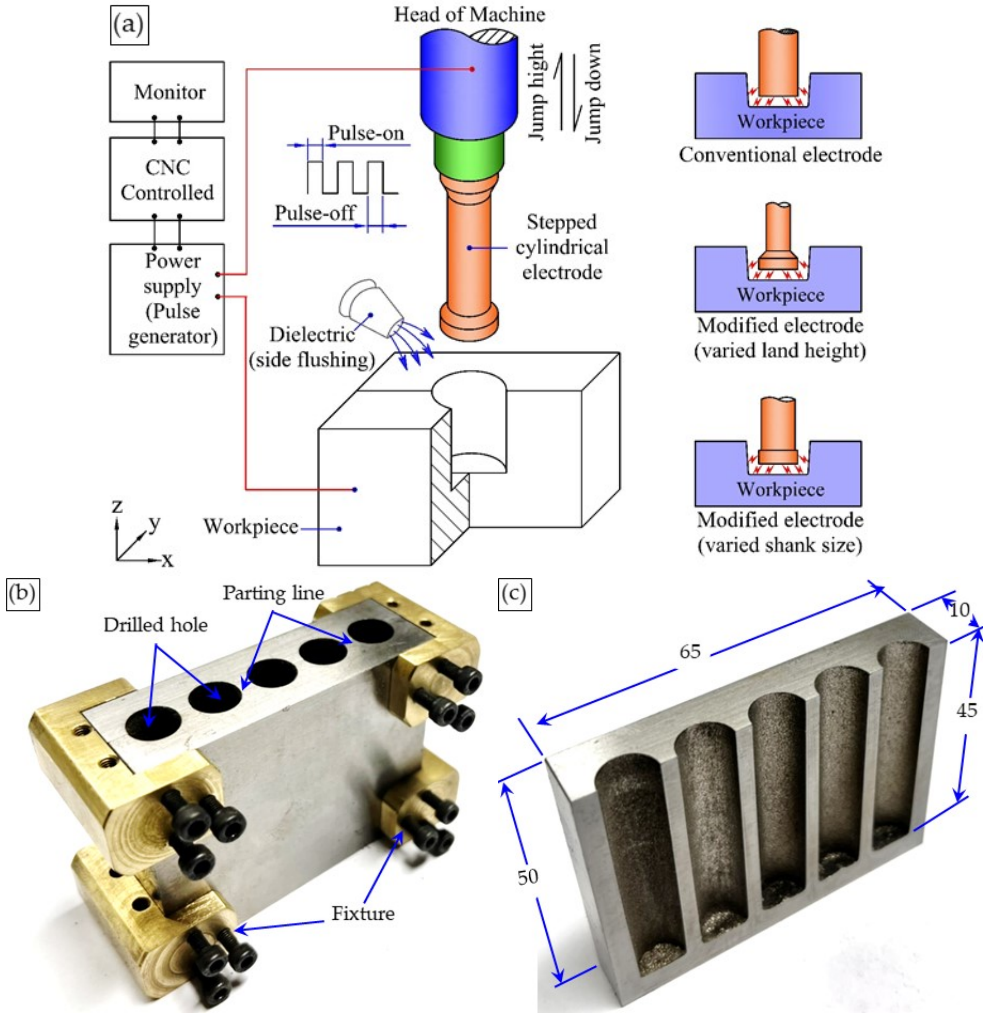

Figure 1 Experimental setup: (a) schematic of the experimental setup; (b) assembled coupled plate with screw clamps; (c) drilled holes in the steel plate

2.2 Electrode design

Electrode designs are in accordance with the flow difference through the narrow flushing channel, which affects the velocities and pressure. Dielectric flushing creates a difference in pressure at the drilled position (Chen et al., 2025). The hole depth influences the drop in

dielectric flushing pressure for conventional electrodes (Kliuev et al., 2018). The concave shape of the electrode reduces debris accumulation with the dielectric fluid's flushing effect (Mao et al., 2020). The shape of the rotating electrode design can improve the machining performance by promoting self-pumping dielectric flushing (Goiogana and Elkaseer, 2019). A cylindrical shape with a uniform cross-sectional area is the conventional electrode design, which is typically used to produce a circular hole in the electrical discharge machining process, as shown in Figure 2. In this study, the cylindrical electrode was modified into different design types through the land height (LH) and shank size (SZ) to evaluate the effects on machining performance. The effects of the land height and shank size on the improvement in machining performance of the shoulder electrode design (stepped 90 degrees, SE) and the relief angle electrode design (stepped 45 degrees, RE) were investigated and compared with those of the conventional electrode. The electrode design was further characterized by the LH into five subdesign parameters of 0.90, 2.25, 4.50, 6.75, and 9.00 mm for the shoulder electrode (SE) and relief angle electrode (RE) with a specified shank size of 4.5 mm, as shown in Figures 2(a) and 2(b), respectively. The selection of the land height was expected to increase the percentage of electrode diameter by 10%, 25%, 50%, 75%, and 100%, respectively, because the side gap strongly affects the accumulation of debris at the bottom of the hole in the gap and sparking region between the electrode and workpiece (Firat and Bozdana, 2025; Mao et al., 2020). The shank size (SZ) of the electrode was further varied into four subdesign diameters of 8.10, 7.20, 6.30, and 5.40 mm for the shoulder electrode (SE) and relief angle electrode (RE), as shown in Figures 2 (c) and 2 (d), respectively. A total of 19 electrode designs, including conventional electrodes, were used to perform the machining tests. All electrode designs were manufactured using an automatic turning machine (EMCOTRONIC TM02). The electrode diameter was controlled to a body size of 9.00 ± 0.002 mm.

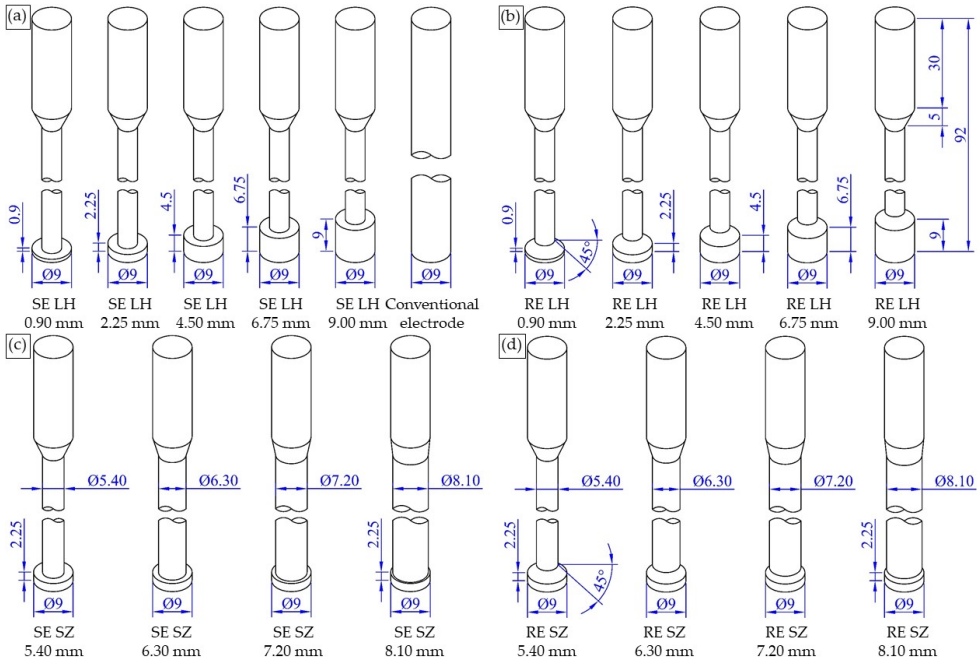

Figure 2 Stepped cylindrical electrode designs: (a) shoulder electrodes with varied land heights (SE LH); (b) relief angle electrodes with varied land heights (RE LH); (c) shoulder electrodes with varied shank sizes (SE SZ); (d) relief angle electrodes with varied shank sizes (RE SZ)

2.3 Experimental procedure

In this experiment, the head of the machine was equipped with a copper electrode with a body diameter of 9 ± 0.002 mm. AISI P20 grade tool steel was used for the 45 mm drilling hole. The top surface of the workpiece served as the zero position for the machining setup. Table 1

summarizes the machining conditions investigated. The electrode polarity was set as an anode (+), and the workpiece material was set as the cathode (-). In accordance with the optimized machining conditions with regard to the highest material removal rate, the discharge current, pulse-on time, and pulse-off time for any experimental testing were fixed at 16 Amp, 150 μs, and 2 μs, respectively (Jamkamon and Janmanee, 2021; Tapadar et al., 2017). The experimental tests were repeated 3 times for each tool design with the new electrode.

Table 1 Experimental conditions used

No.	Machining condition	Value
1	Electrode diameter (mm)	9.00 + 0.002
2	Electrode polarity	+ (anode)
3	Discharge current (Amp)	16.00
4	Pulse-on time (μs)	150
5	Pulse-off time (μs)	2
6	Voltage (V)	150
7	Gap spark (μm)	10
8	Jump height (mm)	2
9	Jump down (s)	2
10	Side flushing flow (Lmin)	1
11	Machining depth (mm)	45

The drilling depth and machining time (MT) were monitored and recorded from the display of the machine by a video camera. The material loss of the workpiece and electrode was determined using a digital balance. Therefore, the MRR can be derived from the volume of work material lost per unit of machining time, as shown in Equation (1). The electrode wear ratio (EWR) can be calculated as the percentage volume of worn electrode per work material loss, as derived by Equation (2) (Barenji et al., 2016). The dimensions of the drilled hole along the machining depth were determined using an optical measuring microscope (Olympus, STM6, Japan), and the quality of the machined surface in terms of arithmetic mean roughness (Ra) was measured using a roughness tester (Mahr, Marsurf PS1, Germany). The evaluation of weight and surface roughness was replicated 3 times for each measurement.

$$MRR = \frac{M_{w1} - M_{w2}}{\rho_w \times MT} \times 10^3 \tag{1}$$

where MRR is the material removal rate (mm^3/min) and M_{w1} and M_{w2} are the weights (g) of the workpiece material before and after machining, respectively. ρ_w is the density of the workpiece material (AISI P20 tool steel, 7.78 g/cm^3), and MT is the machining time (min).

$$EWR = \frac{(M_{t1} - M_{t2})\rho_t}{(M_{w1} - M_{w2})\rho_w} \times 100 \tag{2}$$

where EWR is the electrode wear ratio (%), M_{t1} and M_{t2} are the weights (g) of the tool electrode before and after machining, respectively, and ρt is the density of the copper electrode (8.96 g/cm^3).

3. Results and Discussion

The main focus of this study was the impact of the stepped cylindrical electrode design on enhancing the machinability of the electrical discharge machining procedure for deep hole drilling. The effects of the land height and shank size of the electrode design on the machining performance were assessed in terms of the machining time, material removal rate, and electrode wear ratio. Furthermore, the integrity of the machined hole was analyzed and linked to the drilled hole's diameter and surface roughness (Ra).

3.1 Machining time

Figure 3 shows the experimental results of the machining time with varied land heights for the shoulder and relief angle electrodes. The machining time increased proportionally with the depth of the drilled hole for all electrode designs. The shoulders electrode (SE) design with varied land heights of 0.90, 2.25, 4.50, 6.75, and 9.00 mm for a drilling depth of 45 mm influenced the machining time by approximately 115.13, 128.47, 226.40, 360.15, and 418.88 min, respectively, as shown in Figure 3(a). The machining time of the relief angle electrode design (RE) increased by approximately 118.53, 131.67, 198.72, 316.55, and 376.80 min with increasing land height, as shown in Figure 3(b).

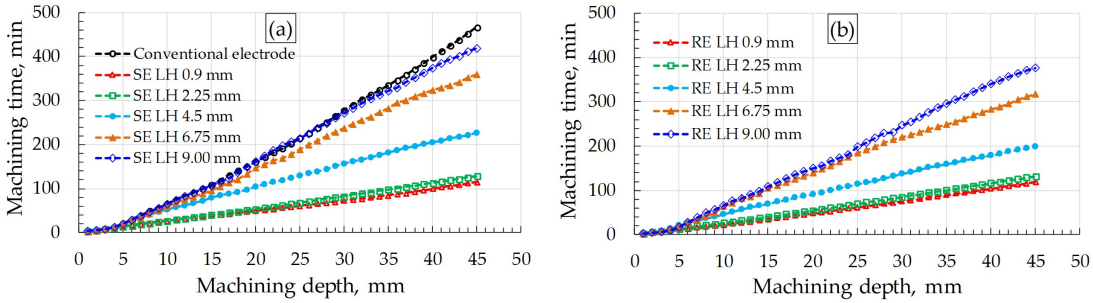

Figure 3 Machining time of the cylindrical electrode design with various land heights: (a) shoulder electrode (SE LH); (b) relief angle electrode (RE LH)

When the land height was increased, the machining time of the relief angle electrode was slightly lower than that of the shoulder electrode. The smaller land height of the electrode resulted in a shorter machining time to finish the drilled hole. Larger land heights resulted in longer machining times and approximately 466.73 min than the results of holes drilled with conventional electrodes. The machining time increased with increasing land height for both electrode designs because the large electrode area easily induced a secondary spark on the drilled hole's sidewall. This resulted from the build-up of debris particles, which decreased the dielectric fluid's resistance (Lo et al., 2019). When the work material in the machining zone was eliminated, the large area of the secondary spark resulted in a low energy density, which required more machining time (Liao et al., 2020; Giridharan and Samuel, 2015). An image of the effects of the secondary spark on the electrode sidewall, which is displayed in Figure 4, supports this hypothesis. The secondary spark area of the electrode sidewall is shown in a darker shade. Thus, the design land height of the electrode body can be adapted to reduce the machining time. The lowest drilling time was related to the highest machining speed of 0.39 mm/min (45 mm/115.13 min). These results are better than those of Rafaqat et al., 2020 (0.35 mm/min (4 mm/11.27 min)) by approximately 11.43%.

Figures 5(a) and (b) show the results of the machining time with various shank sizes (SZ) for the shoulder and relief angle electrode designs. For both electrode designs, the machining time increased with increasing depth of the drilled hole. However, for both the shoulder and relief angle electrode designs, the slope of the machining time against the drilled hole depth for a shank size of 8.1 mm significantly increased when the machining depth exceeded 30 mm. The machining time required to finish the drilled hole for both electrode designs was approximately 125 ± 5 minutes with various shank sizes ranging from 5.4 to 7.2 mm. The modified shank size of the electrode resulted in the greatest decrease in the machining time, which was approximately 73.22%, compared with the conventional shape. In addition, a machining time of approximately 170 ± 5 minutes was required for both electrodes with a shank size of 8.1 mm. This was possibly due to the larger shank size, which resulted in lower clearance between the electrode wall and the drilled hole, leading to the small escape area and the effect of gravity preventing the removal of bubbles and debris particles from the machining zone (Mao et al., 2024; Tanjilul et al., 2017). Differences in electrode body and shank sizes led to debris particles and gas bubbles easily moving out from the machining region because of the large escape area (Figure

6). These results are similar to those of Kumar and Singh, 2019 in that they improved the process performance of electrical discharge drilling with fabricated pathways on the electrode to eliminate debris particles and gas bubbles from the machining area.

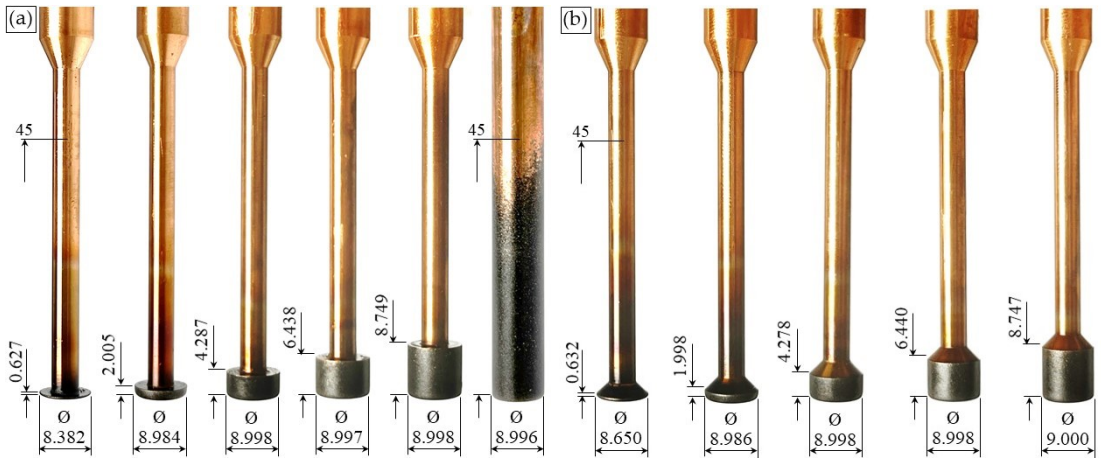

Figure 4 Photographs after secondary sparks occurred on the sidewalls of electrodes with various land heights: (a) varied land height of the shoulder electrode (SE LH); (b) varied land height of the relief angle electrode (RE LH)

EDM systems require low production costs and short machining times (Hasan et al., 2023). The machining times for the stepped cylindrical electrode with a land height of 2.25 mm for both the shoulder and relief angle electrode designs were approximately 72.47% ((100)(466.73–128.47)/466.73)) and 71.78% ((100)(466.73–131.67)/466.73%), respectively, lower than that of the conventional electrode. Therefore, modified electrode designs can improve machining performance without the need for special attachments on machines. This is beneficial for reducing production costs related to a decrease in machining time.

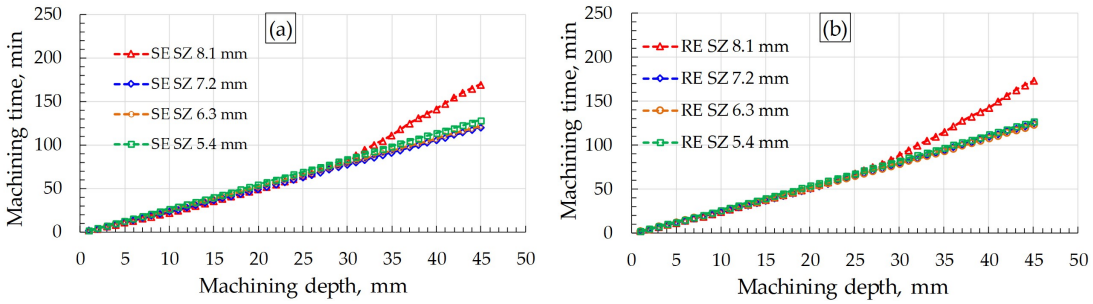

Figure 5 Machining times of the cylindrical electrode designs: (a) shoulder electrode with various shank sizes (SE SZ) and (b) relief angle electrode with various shank sizes (RE SZ)

3.2 Material removal rate (MRR)

The MRR with various land heights for a machining depth of 45 mm is shown in Figure 7(a). The land height of the shoulder and the relief angle of the electrode designs affected the material removal rate. The material removal rate drastically decreased when the land height of the electrode increased for both electrode designs. The greatest improvement in the material removal rate of the shoulder and relief angle electrodes occurred at approximately 277.54% and 269.91%, respectively, for a land height of 0.9 mm compared with conventional machining. The highest material removal rate occurred at the lowest land height because the dielectric fluid was easily transported to the sparking area (Kolli and Kumar, 2015). The dielectric fluid flow through the machining area induced a stable discharge current and eliminated debris particles from the sparking region (Machno et al., 2020; Takezawa et al., 2020). The increase in the clearance between the wall of the drilled hole and the electrode with the reduced shank size

also affected the material removal rate, as shown in Figure 7(b). The largest shank size (8.1 mm) resulted in the lowest material removal rates 17.95 and 17.53 mm^3/min for the shoulder and relief angle electrode designs, respectively. The material removal rate increased when the electrode shank size decreased. The highest material removal rates of approximately 25.06 and 25.20 mm^3/min for the shoulder and relief angle designs, respectively, occurred for the electrode shank size of 7.2 mm. The material removal rate fluctuated slightly when the shank size of the electrode decreased. This was possibly due to the sufficient escape area for debris particle and gas bubble removal from the machining region, leading to reduced short circuits with successful sparking (Ekmekci and Sayar, 2012).

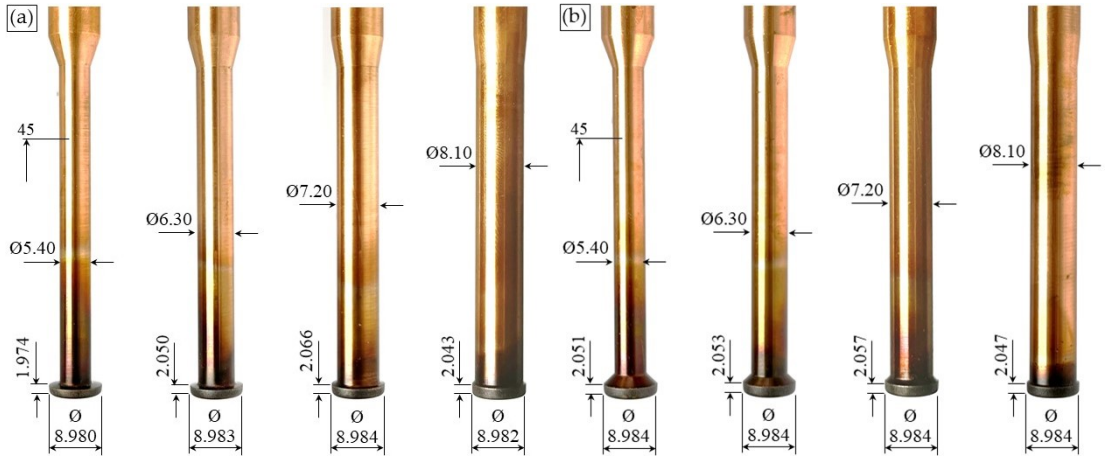

Figure 6 Photographs of the machined electrodes: (a) shoulder electrode with various shank sizes (SE SZ); (b) relief angle electrode with various shank sizes (RE SZ)

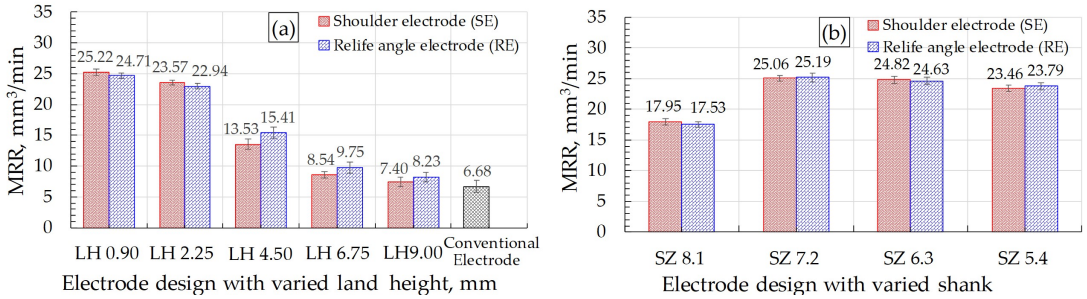

Figure 7 Material removal rates of the shoulder and relief angle electrode designs: (a) material removal rate with varied land heights; (b) material removal rate with varied shank sizes

Regressions of the material removal rate (MRR) as a function of the land height (LH) for the shoulder electrode (SE) and relief angle electrode (RE) are presented in Equations (3) and (4), respectively. The regression model revealed that the material removal rate decreased linearly as the land height increased. The coefficients of determination (R-squared) of the shoulder and relief angle electrodes were 92.75 and 95.85, respectively.

$$MRR_{SE}\,(mm^3/min) = 27.08 - 2.441(LH), \tag{3}$$

$$MRR_{RE}\,(mm^3/min) = 26.63 - 2.228(LH), \tag{4}$$

where MRR_{SE} (mm^3/min) and MRR_{RE} (mm^3/min) are the predicted volume of the material removal rate (mm^3/min) for the shoulder and relief angle electrodes, respectively, and LH is the land height (mm).

The experimental results of the material removal rate for the shoulder and relief angle electrodes present the regression model as a quadratic function with the shank size, as shown

in Equations (5) and (6). The coefficients of determination of the regression model of both the shoulder and relief angle electrodes were 94.14 and 91.66, respectively.

$$MRR_{SE}\,(mm^3/min) = -81.42 + 33.48(SZ^2), \tag{5}$$

$$MRR_{RE}\,(mm^3/min) = -80.42 + 33.39(SZ^2), \tag{6}$$

where MRR_{SE} (mm^3/min) and MRR_{RE} (mm^3/min) are the predicted volume of the material removal rate (mm^3/min) for the shoulder and relief angle electrodes, respectively, and SZ is the shank diameter (mm).

3.3 Electrode wear ratio (EWR)

Figure 8(a) shows the results of the electrode wear ratio with various land heights. The highest electrode wear ratios of 0.63% and 0.57% were observed at a land height of 0.90 mm for the shoulder and relief angle electrodes, respectively. These values are slightly lower than those of the conventional electrodes (0.66%). An increase in the land height of 2.25 mm led to the lowest electrode wear ratio of 0.45%, which slightly increased for both tool designs. This was possibly due to the shortest land height inducing high energy density in the machining area, leading to more erosion on the sidewall and electrode surface because of the small sparking area. In other words, increased land height led to low energy density in the machining region because of a greater area of the secondary spark, resulting in weak electrode tool wear (X. Wang et al., 2020). This can be confirmed by the worn electrode images shown in Figures 4 and 6. The greatest change in the dimension of the worn electrode occurred at the lowest land height. Debris particles and gas bubbles readily escaped from the sparking area because of the increased clearance caused by the smaller shank size of the electrode. As shown in Figure 8(b), this led to a reduced electrode wear ratio with minor volatility and a quicker machining time.

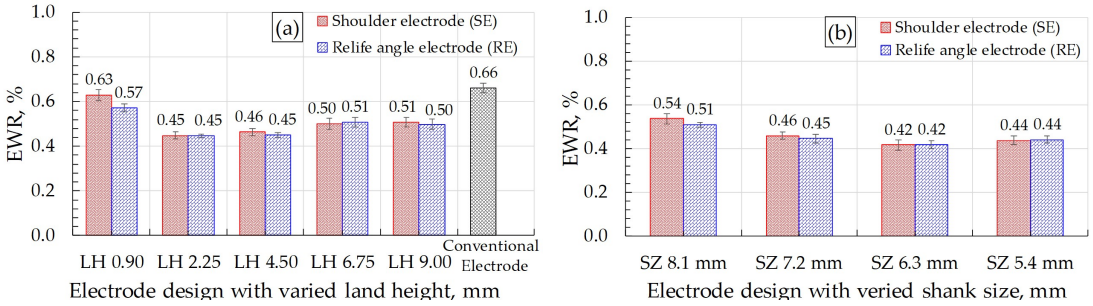

Figure 8 Electrode wear ratio of the shoulder and relief angle electrode designs: (a) electrode wear ratio with varied land heights and (b) electrode wear ratio with varied shank sizes

The volume of the electrode wear ratio was predicted by regression of the cubic and quadratic models when the land height and shank size were controlled for the shoulder and relief angle designs, as presented in Equations (7), (8), (9), and (10), respectively. The cubic regression model's coefficient of determination for varied land heights of the shoulder and relief angle electrodes were 94.29 and 99.24, respectively. The coefficients of determination of the quadratic regression model for the electrode designs with various shank sizes of the shoulder and the relief angle electrodes were 99.76 and 99.56, respectively.

$$EWR_{SE}(\%) = 0.8041 - 0.2440(LH) + 0.04880(LH^2) - 0.002818(LH^3), \tag{7}$$

$$EWR_{RE}(\%) = 0.7094 - 0.1914(LH) - 0.04021(LH^2) - 0.002393(LH^3), \tag{8}$$

$$EWR_{SE}(\%) = 1.585 - 0.3789(SZ) + 0.03086(SZ^2), \tag{9}$$

$$EWR_{RE}(\%) = 1.375 - 0.3067(SZ) + 0.02469(SZ^2), \quad (10)$$

where EWR_{SE} (%) and EWR_{RE} (%) are the predicted electrode wear ratios (%) for the shoulder and relief angle electrodes, respectively. LH and SZ are the land height (mm) and shank size, respectively.

Figure 9 shows the characteristics of tool wear in the bottom face of the electrode. Images were captured using a 3D measuring laser microscope (Olympus, model LEXT OLS 5000). The surface profile of the electrode is represented by the shaded color. Most tool wear occurred on the electrode's bottom surface and edge region. The depth of tool wear on the bottom surface of the tool slightly increased with increasing land height for the shoulder and relief angle electrodes, as shown in Figure 9(a). This occurred because the area against the electrode sidewall and the drilled hole, where the dielectric fluid barely passed through the sparking area, increased as the land height increased. As a result, debris particles accumulate in the dielectric fluid, causing turbulent flushing of the dielectric fluid to produce secondary sparks at the bottom section of the machining area (Voigt and Peuker, 2022). The irregular wear on the surface increased slightly with increasing shank size. However, the shoulder and relief angle designs had little effect on the tool wear characteristics with varying shank sizes, as shown in Figure 9(b).

Figures 10 and 11 show the contour plots of land height (LH) versus material removal rate (MRR) and electrode wear ratio (EWR) for the shoulder electrode (SE) and relief angle electrode (RE), respectively. Electrode wear increased when the land height was less than 2.0 mm. The material removal rate decreased with increasing land height. However, both the shoulder and relief angle electrodes promoted the highest material rate with the lowest electrode wear ratio when the land height ranged from 2 - 4 mm.

Figures 12 and 13 present contour plots of the shank size (SZ) versus the material removal rate (MRR) and electrode wear ratio (EWR) for the shoulder electrode (SE) and relief angle electrode (RE), respectively. Large shank size decreased the material removal rate and increased the electrode wear ratio. However, high machining performance occurred when the shank size was controlled in the range of 6.0 - 6.5 mm, as indicated by the high material removal rate and low electrode wear ratio. Therefore, the design of a sufficient area for debris particle and bubble escape from the machining region can improve the machinability of electrical discharge machining (Chen et al., 2025; Wei et al., 2025).

3.4 Integrity of the machined surface

In this work, the diameter of the electrode design was 9.00 ± 0.002 mm. The integrity of the machined surface was investigated in terms of the diameter and roughness of the drilled hole. The experimental results for the diameter of the drilled hole were usually larger than the diameter of the electrode because of the clearance of the spark gap, as shown in Figure 14. The results show that a short land height of 0.9 mm led to a decrease in the dimensions of the drilled hole with increasing machining depth for both the shoulder and the relief angle electrode designs, as shown in Figure 14(a) and 14(b), respectively. This occurred because the concentrated secondary spark in the small area accelerated tool wear and resulted in a dimensional change with increasing depth of drilling (Zhu et al., 2025). Compared with the relief angle electrode design, the shoulder electrode design's reduced material volume caused a more significant change in dimension. The drilled hole diameter increased as a larger land height of electrode. This occurred because a larger secondary spark was produced by more debris particles merging in the space between the electrode sidewall and the drilled hole, which decreased the dielectric fluid resistance and increased the sparking gap.

This can be confirmed by the results of the dimensional concavity of the drilled hole, which increased with the land height of the electrode for both the shoulder and the relief angle designs, as shown in Figure 14. However, the concave shape of the drilled hole for all the modified electrodes was lower than that for conventional machining. The highest quality of the drilled holes in terms of the average gap clearance was 0.188 mm ((9.359-8.984)/2) and 0.180 mm

((9.347-8.986)/2), which increased with a controlled land height of 2.25 mm for both the shoulder and the relief angle electrode designs, respectively. A quantitative comparison revealed that the gap clearance with the relief angle electrode was lower than the optimal condition of previous research by approximately 8.16% ((100)(0.196-0.180)/0.196)). Notably, the gap clearance under optimal conditions for multi-aperture inner flushing was reported to be 0.196 mm (Chuvaree and Kanlayasiri, 2021).

Figure 15 shows the diameter of the drilled hole with respect to the machining depth for various electrode shanks. The diameter of the drilled hole decreased slightly with the shank size for the shoulder electrode design, as shown in Figure 15(a). However, the diameter of the hole drilled using the relief angle electrode changed slightly less with decreasing electrode shank size, as shown in Figure 15(b). This is possibly due to the erosion effect of material debris particles flowing out from the machining area via dielectric flushing and gas bubbles during the sparking cycle (Ablyaz et al., 2023). The discharge current was stopped during the jump height cycle, leading to the reversal of the dielectric fluid flow to the machining area through the gap between the electrode's sidewall and the workpiece. The debris particles blending in the dielectric fluid accumulate on the electrode shoulder, which can be moved back to produce a secondary spark on the sidewall of the drilled hole. On the other hand, the slope surface of the electrode in the relief angle design induced a stable flow of debris particles and bubbles from the sparking region (Cetin et al., 2004). Therefore, the design of the relief angle electrode was more appropriate than that of the shoulder electrode because the dimensions of the drilled hole were close to the electrode's negligible shank size.

Figure 16 shows the surface roughness results for the sidewall of the drilled hole. The roughness of the machined surface was measured. The shortest land height of 0.90 mm for both the shoulder and relief angle electrodes represented the highest arithmetic mean roughness (Ra $\approx$ 11.50 μm), as shown in Figure 16(a). At a land height of 2.25 mm, the roughness of the machined surface significantly decreased. The roughness levels of the machined surface were higher at lower land heights (2.25-9.00 mm), with little variation between 4.10 and 5.50 μm. The lowest roughness level of the machined surface, 3.54 μm, occurred for the conventional electrode. This phenomenon was possibly due to the small area on the side surface of the electrode affecting high-energy sparking in the machining area, causing more damage to the workpiece. The distribution of spark energy over a wide area decreased the roughness of the machined surface, which was caused by the secondary spark on the sidewall when the surface area of the electrode increased with increasing land height. The secondary spark on the side surface of the electrode reduced the workpiece recasting peak region and debris particle accumulation in the valley area. This can be confirmed by the photograph and profile of the machined surface shown in Figure 16(b).

The number of cutoffs and the measuring length of the sample were 5 periods and 0.8 mm. The photographs represent the workpiece recasting of metal and debris particle accumulation on the machined surface as brightness and dark shading. However, the bright area was present only in the SE LH (9.00 mm), RE LH (9.00 mm), and conventional electrode images. Additionally, the increased land height reduced the peaks and valleys of surface profile on the sidewall of the drilled hole. Thus, it can be concluded that the adequate land height of electrode design resulted in a better quality of the machined surface, which was similar to that of conventional cutting.

4. Conclusions

The machining time increased with the depth of the drilled hole for all electrode designs. The lower land height and smaller shank size of the electrode resulted in shorter machining times for both the shoulder and relief angle electrode designs. The improvement in machining time for the relief angle design compared with that of a conventional electrode was approximately 74.60%, 71.78%, 57.42%, 32.17%, and 19.26% for varied land heights of 0.90, 2.25, 4.50, 6.75, and 9.00 mm, respectively. The material removal rate decreased when the land height of the electrode increased because a greater area induced a secondary spark on the sidewall of the

electrode and workpiece. The greatest improvements in the material removal rate compared with conventional machining were 269.91, 243.41, 130.68, 45.95, and 23.20%, which occurred with varied land heights for the relief angle designs of 0.90, 2.25, 4.50, 6.75, and 9.00 mm, respectively. The contour plots presented the highest material removal rate and lowest electrode wear ratio with the land height and sank size of approximately 2 - 4 mm and 6.0 - 6.5 mm, respectively. In addition, the relief angle design of the electrode is more appropriate than that of a shoulder electrode because the diameter of the drilled hole is close to negligible for the shank size of the electrode, leading to an increase in machining precision.

Acknowledgements

For financial support of this study, the authors would like to thank Thailand Science Research and Innovation (TSRI) and Rajamangala University of Technology Krungthep." with "For financial support of this study, the authors would like to thank Thailand Science Research and Innovation (TSRI), Project code: TSRI 185788.

Author Contributions

Kamonpong Jamkamon: Conceptualized and designed the study, developed the methodology, conducted the experiments, performed data analysis, and drafted the manuscript. Pichai Janmanee: Conducted experiments and contributed to data collection, assisted in manuscript drafting, Niwat Mookam: Contributed to methodology development, assisted in experimental setup, and participated in data collection. Suppawat Chuvaree: Proposed the research idea, supervised the project, contributed to conceptualization, assisted in manuscript drafting, provided critical revisions and editing, and served as the corresponding author.

Conflict of Interest

The authors declare no conflicts of interest.

Supplementary Materials

Figure 9-Figure 16 at the supplementary file.

References

Ablyaz, T. R., Shlykov, E. S., & Muratov, K. R. (2023). Modeling of edm process flushing mechanism. *Materials*, *16*(11), 4158. https://doi.org/10.3390/ma16114158

Aghdeab, S. H., Shwaish, R. R., & Salman, T. M. (2021). Effect of input parameters on mrr and ewr for tool steel aisi l2 by electric discharge machine (edm). *IOP Conference Series: Materials Science and Engineering*, *1076*(1), 012071. https://doi.org/10.1088/1757-899x/1076/1/012071

Ahmed, A., Boban, J., & Rahman, M. (2021). Novel edm deep hole drilling strategy using tubular electrode with orifice. *CIRP Annals*, *70*(1), 151–154. https://doi.org/10.1016/j.cirp.2021.04.004

Barenji, R. V., Pourasl, H. H., & Khojastehnezhad, V. M. (2016). Electrical discharge machining of the aisi d6 tool steel: Prediction and modelling of the material removal rate and tool wear ratio. *Precision Engineering*, *45*, 435–444. https://doi.org/10.1016/j.precisioneng.2016.01.012

Cetin, S., Okada, A., & Uno, Y. (2004). Effect of debris distribution on wall concavity in deep-hole edm. *JSME International Journal Series C*, *47*(2), 553–559. https://doi.org/10.1299/jsmec.47.553

Chen, Y., Mi, D., & Natsu, W. (2025). A method to enhance the depth-to-diameter ratio of micro-holes drilled with edm using the pressure difference created at the hole en-

trance. *International Journal of Precision Engineering and Manufacturing*, *26*(3), 727–736. https://doi.org/10.1007/s12541-024-01152-y

Chuvaree, S., & Kanlayasiri, K. (2021). Effects of side flushing and multi-aperture inner flushing on characteristics of electrical discharge machining macro deep holes. *Metals*, *11*(1), 148. https://doi.org/10.3390/met11010148

Dhakar, K., Kumar, R., Katheria, A., Nagdeve, L., & Kumar, H. (2022). Effect of various dielectric fluids on electric discharge machining (edm): A review. *Journal of the Brazilian Society of Mechanical Sciences and Engineering*, *44*(10), 487. https://doi.org/10.1007/s40430-022-03778-3

Dwivedi, A. P., & Choudhury, S. K. (2017). Estimation of recast layer thickness in rotary tool edm process for machining aisi d3 tool steel. *Materials Today: Proceedings*, *4*(10), 10816–10822. https://doi.org/10.1016/j.matpr.2017.08.033

Ekmekci, B., & Sayar, A. (2012). Debris and consequences in micro electric discharge machining of micro-holes. *International Journal of Machine Tools and Manufacture*, *65*, 58–67. https://doi.org/10.1016/j.ijmachtools.2012.10.003

Firat, A. G., & Bozdana, A. T. (2025). Experimental study on effect of geometry and material of tubular electrode in electrical discharge drilling of tungsten carbide. *Physica Scripta*, *100*(7), 075017. https://doi.org/10.1088/1402-4896/ade2a1

Giridharan, A., & Samuel, G. (2015). Analysis on the effect of discharge energy on machining characteristics of wire electrical discharge turning process. *Proceedings of the Institution of Mechanical Engineers, Part B: Journal of Engineering Manufacture*, *230*(11), 2064–2081. https://doi.org/10.1177/0954405415615732

Goiogana, M., & Elkaseer, A. (2019). Self-flushing in edm drilling of ti6al4v using rotating shaped electrodes. *Materials*, *12*(6), 989. https://doi.org/10.3390/ma12060989

Hasan, M. M., Saleh, T., Sophian, A., Rahman, M. A., Huang, T., & Mohamed Ali, M. S. (2023). Experimental modeling techniques in electrical discharge machining (edm): A review. *The International Journal of Advanced Manufacturing Technology*, *127*(5), 2125–2150. https://doi.org/10.1007/s00170-023-11603-x

Jamkamon, K., & Janmanee, P. (2021). Improving machining performance for deep hole drilling in the electrical discharge machining process using a step cylindrical electrode. *Applied Sciences*, *11*(5), 2084. https://doi.org/10.3390/app11052084

Kliuev, M., Baumgart, C., Büttner, H., & Wegener, K. (2018). Flushing velocity observations and analysis during edm drilling. *Procedia CIRP*, *77*, 590–593. https://doi.org/10.1016/j.procir.2018.08.210

Kolli, M., & Kumar, A. (2015). Effect of dielectric fluid with surfactant and graphite powder on electrical discharge machining of titanium alloy using taguchi method. *Engineering Science and Technology, an International Journal*, *18*(4), 524–535. https://doi.org/10.1016/j.jestch.2015.03.009

Kumar, R., & Singh, I. (2018). Productivity improvement of micro edm process by improvised tool. *Precision Engineering*, *51*, 529–535. https://doi.org/10.1016/j.precisioneng.2017.10.008

Kumar, R., & Singh, I. (2019). A modified electrode design for improving process performance of electric discharge drilling. *Journal of Materials Processing Technology*, *264*, 211–219. https://doi.org/10.1016/j.jmatprotec.2018.09.014

Liao, Z., La Monaca, A., Murray, J., Speidel, A., Ushmaev, D., Clare, A., Axinte, D., & M'Saoubi, R. (2020). Surface integrity in metal machining - part i: Fundamentals of surface characteristics and formation mechanisms. *International Journal of Machine Tools and Manufacture*, *162*, 103687. https://doi.org/10.1016/j.ijmachtools.2020.103687

Lo, J. S., Deng, C. S., Jiang, C. T., & Lu, C. H. (2019). Slotted electrodes for the improvement of machining performances in edm drilling. *Journal of the Chinese Institute of Engineers*, *42*(5), 401–410. https://doi.org/10.1080/02533839.2019.1599300

Machno, M., Bogucki, R., Szkoda, M., & Bizoń, W. (2020). Impact of the deionized water on making high aspect ratio holes in the inconel 718 alloy with the use of electrical discharge drilling. *Materials*, *13*(6), 1476. https://doi.org/10.3390/ma13061476

Mao, X., Wang, X., Li, C., Mo, J., & Ding, S. (2020). Effects of stepped cylindrical electrode in electrical discharge machining of blind holes. *The International Journal of Advanced Manufacturing Technology*, *110*(5–6), 1457–1469. https://doi.org/10.1007/s00170-020-05941-3

Mao, X., Wu, G., Tran, M., Yi, S., & Ding, S. (2024). Electrical discharge drilling of blind holes with injection flushing dielectric and stepped electrodes. *The International Journal of Advanced Manufacturing Technology*, *132*(1–2), 495–511. https://doi.org/10.1007/s00170-024-13396-z

Mookam, N., Sunasuan, P., Madsa, T., Muangnoy, P., & Chuvaree, S. (2021). Effects of graphite and boron carbide powders mixed into dielectric fluid on electrical discharge machining of skd 11 tool steel. *Arabian Journal for Science and Engineering*, *46*(3), 2553–2563. https://doi.org/10.1007/s13369-020-05156-4

Mufti, N. A., Rafaqat, M., Ahmed, N., Saleem, M. Q., Hussain, A., & Al-Ahamri, A. M. (2020). Improving the performance of edm through relief-angled tool designs. *Applied Sciences*, *10*(7), 2432. https://doi.org/10.3390/app10072432

Ni, H., Gong, H., Dong, Y. H., Fang, F. Z., & Wang, Y. (2017). A comparative investigation on hybrid edm for drilling small deep holes. *The International Journal of Advanced Manufacturing Technology*, *95*(1–4), 1465–1472. https://doi.org/10.1007/s00170-017-1282-1

Priyadarshini, M., Behera, A., Biswas, C. K., & Rajak, D. K. (2022). Experimental analysis and mechanical characterization of aisi p20 tool steel through heat-treatment process. *Journal of Bio- and Tribo-Corrosion*, *8*(1). https://doi.org/10.1007/s40735-021-00607-3

Rafaqat, M., Mufti, N. A., Ahmed, N., Alahmari, A. M., & Hussain, A. (2020). Edm of d2 steel: Performance comparison of edm die sinking electrode designs. *Applied Sciences*, *10*(21), 7411. https://doi.org/10.3390/app10217411

Straka, L., & Hašová, S. (2018). Optimization of material removal rate and tool wear rate of cu electrode in die-sinking edm of tool steel. *The International Journal of Advanced Manufacturing Technology*, *97*(5–8), 2647–2654. https://doi.org/10.1007/s00170-018-2150-3

Takezawa, H., Toyoda, H., & Yuasa, K. (2020). Small-hole edm using grooved pipe electrode. *Procedia CIRP*, *95*, 545–549. https://doi.org/10.1016/j.procir.2020.03.135

Tanjilul, M., Ahmed, A., Kumar, A. S., & Rahman, M. (2017). A study on edm debris particle size and flushing mechanism for efficient debris removal in edm-drilling of inconel 718. *Journal of Materials Processing Technology*, *255*, 263–274. https://doi.org/10.1016/j.jmatprotec.2017.12.016

Tapadar, J., Thakur, R., Chetia, P., Tamang, S. K., & Samanta, S. (2017). Modeling of wedm parameters while machining mg-sic metal matrix composite. *International Journal of Technology*, *8*(5), 878. https://doi.org/10.14716/ijtech.v8i5.870

Voigt, O., & Peuker, U. A. (2022). Suitability of eroded particles from die-sink electro discharge machining for additive manufacturing—review, characterization and processing. *Metals*, *12*(9), 1447. https://doi.org/10.3390/met12091447

Wang, J., Han, F., Cheng, G., & Zhao, F. (2012). Debris and bubble movements during electrical discharge machining. *International Journal of Machine Tools and Manufacture*, *58*, 11–18. https://doi.org/10.1016/j.ijmachtools.2012.02.004

Wang, X., Yi, S., Guo, H., Li, C., & Ding, S. (2020). Erosion characteristics of electrical discharge machining using graphene powder in deionized water as dielectric. *The International Journal of Advanced Manufacturing Technology*, *108*(1–2), 357–368. https://doi.org/10.1007/s00170-020-05405-8

Wei, T., Duan, X., Yang, X., Li, G., Han, F., Feng, Y., Wang, X., & Ding, S. (2025). Bubbles and debris in electrical discharge machining: A review. *The International Journal of Advanced Manufacturing Technology*, *136*(5), 1933–1965. https://doi.org/10.1007/s00170-024-14915-8

Zhu, X., Wei, T., Li, S., Li, G., & Ding, S. (2025). Multi-channel electrical discharge machining of ti-6al-4v enabled by semiconductor potential differences. *Micromachines*, *16*(2), 147. https://doi.org/10.3390/mi16020147